*Парусов А.А., Шарапов Р.Р.* Теоретическое и экспериментальное исследование аэродинамических параметров скоростного пассажирского лифта с обтекателем специальной формы // Транспортное, горное и строительное машиностроение: наука и производство. – 2026. – № 40. – С. 36-46.

УДК 621.876.114 https://doi.org/10.26160/2658-3305-2026-40-36-46

# ТЕОРЕТИЧЕСКОЕ И ЭКСПЕРИМЕНТАЛЬНОЕ ИССЛЕДОВАНИЕ АЭРОДИНАМИЧЕСКИХ ПАРАМЕТРОВ СКОРОСТНОГО ПАССАЖИРСКОГО ЛИФТА С ОБТЕКАТЕЛЕМ СПЕЦИАЛЬНОЙ ФОРМЫ

***Парусов А.А., Шарапов Р.Р.***

*Национальный исследовательский Московский государственный строительный университет, Москва*

**Ключевые слова:** скоростной пассажирский лифт, аэродинамика кабины лифта, CFD-моделирование аэродинамических процессов, обтекатель кабины лифта, экспериментальные исследования скоростного лифта, шум и вибрация.

**Аннотация.** Работа высокоскоростных канатных пассажирских лифтов в ограниченном пространстве лифтовой шахты тесно связана с возникновением различных сложных аэродинамических явлений. К ним относятся: развитие турбулентных воздушных потоков с изменяющимися во времени и пространстве градиентами давления и скорости; вихревые потоки, сопровождающиеся отрывом от поверхности обтекаемого тела, а также выраженные колебательные процессы. Совокупное воздействие этих факторов приводит к появлению шума и вибрации во время движения кабины, что ухудшает комфорт пассажиров лифта. Авторами была разработана математическая модель аэродинамических процессов в лифтовой шахте на основе уравнений Навье–Стокса, усредненных по Рейнольдсу (RANS), которые после приведения к транспортной форме были использованы для численного моделирования в программной среде Ansys Fluent. На основе численного анализа реального высокоскоростного лифта из пяти предложенных геометрий обтекателя была выбрана одна конфигурация, обеспечивающая оптимальный баланс между достижимыми аэродинамическими характеристиками и технической осуществимостью промышленного производства. Данная конфигурация позволила снизить коэффициент сопротивления на 41%, уменьшить зону рециркуляции на 54% и снизить амплитуду давления на 97,65 Па. С использованием результатов моделирования в качестве эталона были проведены экспериментальные исследования предложенной конструкции обтекателя, которые подтвердили численные прогнозы и продемонстрировали эффективность предложенного решения с расхождением, не превышающим 10%.

# THEORETICAL AND EXPERIMENTAL INVESTIGATION OF THE AERODYNAMIC PARAMETERS OF A HIGH-SPEED PASSENGER ELEVATOR EQUIPPED WITH A FAIRING OF A SPECIAL SHAPE

***Parusov A.A., Sharapov R.R.***

*Moscow State University of Civil Engineering (National Research University), Moscow*

**Keywords:** high-speed passenger lift, lift car aerodynamics, CFD-modelling of aerodynamic processes, lift car fairing, experimental studies of high-speed lifts, noise and vibration.

**Abstract.** The operation of high-speed rope-driven passenger elevators within the confined space of an elevator shaft is strongly associated with the occurrence of various complex aerodynamic phenomena. These include the development of turbulent air flows with spatially and temporally varying pressure and velocity gradients, flow vortices accompanied by separation from the surface of the streamlined body, as well as pronounced oscillatory responses. The combined action of these factors gives rise to noise and vibration during car motion, thereby impairing ride comfort for elevator users. A mathematical model of the aerodynamic processes in the elevator shaft was developed by the authors on the basis of the Reynolds-averaged Navier–Stokes (RANS) equations, which, after being cast into transport form, were employed for numerical simulations in the Ansys Fluent software environment. Based on the numerical analysis of a real high-speed elevator, one configuration was selected from five proposed fairing geometries, providing an optimal balance between the achievable aerodynamic performance and the technical feasibility of industrial manufacturing. This configuration enabled a 41% reduction in the drag coefficient, a 54% decrease in the recirculation zone, and a reduction of the pressure amplitude by 97.65 Pa. Using the simulation results as a reference, experimental investigations of the proposed fairing design were carried out, which confirmed the numerical predictions and demonstrated the effectiveness of the proposed solution, with a discrepancy not exceeding 10%.

## 1. Introduction

Modern civil and industrial construction is characterized by accelerating urbanization of large cities and megacities, with a pronounced trend toward high-rise development, which, in turn, is driven by the high cost and limited size of land plots. An integral part of any multi-storey building is its vertical transportation systems. Elevator systems are intended to provide comfortable and safe movement of passengers between floors, which poses a challenge to researchers and engineers worldwide in terms of developing new, more compact, advanced, and high-speed systems.

At the turn of the 21st century, interest in high-rise buildings and skyscrapers with heights exceeding 150 m has increased significantly. Such unique buildings are subject to special requirements both at the architectural and structural design stage and in the development of elevator systems. High-speed elevators with rated speeds starting from 3–4 m/s exhibit substantial design and operational differences from other elevator groups and therefore require separate consideration from both a technical and a functional perspective [1].

Nevertheless, the analysis of a number of international and national standards of leading elevator-manufacturing countries, as well as up-to-date scientific studies and technical and operational documentation, has shown that high-speed elevators are currently, for the most part, treated on a par with conventional medium- and low-speed elevators. No specific requirements are defined for the shafts of high-speed elevators, nor are additional measures stipulated to ensure safety and to mitigate adverse factors affecting equipment users.

At the same time, as indicated by a range of relevant scientific investigations and technical descriptions of high-speed elevators, at the early stages of high-speed elevator development, a large number of assumptions were introduced owing to the lack of sufficient engineering and technical background. Subsequently, some of these assumptions – including unaccounted operational loads and impacts – resulted in systematic issues, thereby necessitating a revision of previously adopted approaches and the search for new solutions in the design, manufacturing, and operation of such systems.

One of the most pronounced adverse factors in the operation of high-speed elevators, frequently reported by users, is noise and vibration inside the elevator car [2]. Efforts to address this issue have led to the development of modern sheaves made of polymer materials, the introduction of new car and counterweight guide shoes with spring-loaded rubberized rollers, as well as various types of vibration dampers and sound-insulating materials. Nevertheless, the problem of noise and vibration generated during car motion still lacks a single, universally effective solution.

Thus, it can be concluded that the investigation of the aerodynamics of high-speed elevators and the development of methods for reducing the aerodynamic loads acting on the elevator car constitute a pertinent research problem. This problem is fully aligned with the current interests of the scientific and engineering community in the field of advancing vertical transportation systems within modern science and technology.

As noted above, in recent decades developers have shown increasing interest in the construction of unique high-rise buildings. This trend has led to a growing focus on the investigation of structural and functional parameters of unique high-speed elevators. With regard to the aerodynamics of high-speed elevators, only a relatively narrow body of research can be identified.

A group of researchers from South Korea [3] investigated the aerodynamic characteristics of a high-speed train running in open terrain. The authors modeled the external flow field around the train using direct numerical simulation (DNS). Based on a wavenumber-frequency analysis of pressure fluctuations, the surface pressure signal was decomposed into compressible and incompressible components, i.e., into hydrodynamic and acoustic contributions to the surface pressure fluctuations. As a result, the mechanism of interaction between the airflow and a body moving at high speed was clarified, in particular the power spectral levels of the surface pressure. This study makes it possible to draw conclusions regarding the nature of the interaction of aerodynamic flows when using direct numerical simulation methods. However, it does not address the motion of a body in a confined space, such as an elevator shaft, and it considers operating speeds that are an order of magnitude higher than those typical of elevator systems.

Researchers in the United Kingdom have examined the piston effect in underground railway tunnels [4]. Their work quantified the influence of the aerodynamic profile formed between the streamlined body and the tunnel walls. Based on a two-dimensional mathematical model, validated experimentally, it was shown that varying the angle of attack of the aerodynamic profile can change the volume of displaced air by up to 8% without increasing the aerodynamic work. Another important finding was the identification of flow separation and the prediction of separation locations depending on the shape of the streamlined body.

The studies by Pierre Ricco, Arturo Baron, and Paolo Molteni [5] are aimed at determining the characteristics of the airflow as a function of the blockage ratio, defined as the ratio between the shape and transverse dimensions of the streamlined body and the tunnel cross-section, taking into account viscous effects. In addition, they determined how aerodynamic parameters vary with the length of the streamlined body, which is associated with the influence of the low-pressure region in the rear part of the body on its front part. The authors argue that even when the degree of blockage in front of the body is reduced, that is, when the lateral gaps become larger, a significant pressure level and recirculation zones are still maintained.

According to a number of studies on the aerodynamic parameters of high-speed trains, both in open environments and, in particular, within fully enclosed tunnels, the shape of the streamlined body and the blockage ratio - defined as the ratio of the cross-sectional area of the body to the cross-sectional area of the tunnel through which it moves – are shown to have a decisive influence on the aerodynamic response. However, unlike high-speed trains, elevator shafts accommodate a large amount of additional equipment, which affects the airflow pattern and complicates the experimental validation of numerical predictions. It is also important to emphasize the differences in blockage ratios and operating speed ranges.

Directly in the field of high-speed elevators, relatively few studies have been published to date. Among them, the fundamental work of Hong-lei Bai, Gongxin Shen, and Albert So, published in 2005 [6], presented numerical simulations of aerodynamic processes in a high-speed elevator shaft, explicitly accounting for the blockage ratio. The authors noted that, similarly to high-speed train studies, when the elevator car moves within a confined shaft, comparable aerodynamic phenomena are observed, and the flow profiles depend both on the blockage ratio and on the shape of the car itself. However, that study did not provide a detailed characterization of the flow in the lateral gaps between the streamlined body and the shaft, nor did it include parameters of the wake vortex structure.

More recent research from China [7-9] focuses on the influence of the shape of the upper part of the elevator car on aerodynamic loads and airflow characteristics. The researchers presented numerical simulation results for several roof fairing configurations and analyzed the dependence of the car’s drag on the edge rounding radii of a three-sided fairing. An important contribution of this work is the identification of an optimal three-dimensional computational mesh configuration for numerical simulations, as well as the characterization of the flow within the lateral clearances. However, experimental validation was carried out only for instantaneous pressure at a single point on the car, which is insufficient for a comprehensive verification of the numerical results.

The main objectives of the present study, taking into account the analysis of previously published research, are as follows: to develop a mathematical model of the aerodynamic processes occurring in the shaft of a high-speed elevator, to perform numerical simulations of these processes based on a specific commercially produced high-speed elevator model, to determine the optimal shape of the elevator car fairing, and to carry out experimental validation of the numerical results obtained.

## 2. Modelling of aerodynamic processes

### *2.1. Mathematical modelling*

Mathematical modeling of the airflow within the shaft of a high-speed passenger elevator is based on the conservation laws of mass and momentum for a viscous fluid. The investigated range of car speeds for a high-speed elevator is 4-15 m/s, which corresponds to Mach numbers up to about

0.3. At such Mach numbers, the density variation does not exceed approximately 5%, which allows the air in the elevator shaft to be treated as an incompressible fluid with constant density at each material point without a significant loss of accuracy in the calculations. Under the incompressible-flow assumption, the motion of air can be described by the continuity equation in the form of volumetric flow-rate conservation together with the Navier-Stokes equations for an incompressible flow [10]. Physically, the continuity equation expresses the fact that the mass of fluid within a control volume can increase or decrease only due to the net mass flux across the control surface. One of the fundamental tasks in the modeling process is to determine the characteristics of the airflow, which may be either laminar or turbulent and therefore require different approaches to their assessment. As the flow velocity exceeds a certain critical value, the initially ordered (laminar) flow undergoes transition to a turbulent regime. Turbulent flows are intrinsically unsteady, with characteristic unsteadiness scales spanning a wide range. The ratio between inertial and viscous forces is quantitatively expressed by the Reynolds number, whose critical value defines the onset of transition from laminar to turbulent flow as

$$\mathrm{Re} = \frac{\rho V L}{\mu}, \tag{1}$$

where $\rho$ – fluid density, $\mathrm{kgm}^{-3}$; $V$ – characteristic flow velocity, m/s; $L$ – characteristic length, e.g. gap width or overall car length, m; $\mu$ – dynamic viscosity, $\mathrm{kgm}^{-1}\mathrm{s}^{-1}$.

For Reynolds numbers Re>>1, the flow is turbulent (inertial effects dominate over viscous effects), whereas for Re<<1, the flow remains laminar. Turbulent flows can be characterized by the presence of fluctuations (chaotic pulsations) in velocity, pressure, and other quantities [11]. The spectrum of spatial and temporal scales associated with these fluctuations is quite broad and conventionally includes three types of eddies:

– Large-scale eddies, comparable in size to the elevator car and containing the major part of the turbulent kinetic energy.

– Intermediate-scale eddies, whose characteristic size gradually decreases and which transfer energy toward smaller scales.

– Kolmogorov microscale eddies, which dissipate turbulent kinetic energy into heat due to viscous friction.

Using the Navier-Stokes equations written in index notation, it is possible to describe the instantaneous motion of an incompressible fluid as

$$\frac{\partial u_i}{\partial t} + u_{ij}\frac{\partial u_i}{\partial x_j} = -\frac{1}{\rho}\frac{\partial p}{\partial x_i} + \vartheta\frac{\partial^2 u_i}{\partial x_j \partial x_j}, \tag{2}$$

where $\vartheta$ – kinematic viscosity, $\mathrm{m}^2/\mathrm{s}$; $u_i$ – average value of turbulent velocity, $\mathrm{ms}^{-1}$; $x_i$, $x_j$ – coordinate components.

Nevertheless, direct numerical simulation (DNS) of the Navier-Stokes equations (2), introduced above, may require an extremely fine computational mesh (on the order of 109-1010 cells) in order to resolve all turbulent scales down to the smallest eddies (from order 1 m to $10^{-6}$ m). A similar restriction arises when selecting the time step for numerical time integration ($10^{-6}$), which is necessary to accurately capture high-frequency pressure and velocity fluctuations. Under such conditions, obtaining a solution would demand enormous computational resources, exceeding the capabilities of modern supercomputers, which can perform DNS only for the simplest geometries and over very long wall-clock times (on the order of months). Consequently, the use of DNS is severely limited in engineering practice.

To address the present problem, a more practical approach is adopted, based on time-averaging of the governing equations. This approach filters out small-scale fluctuations from the solution, allows one to work with mean velocity and pressure fields, employ coarser computational grids, and obtain results within significantly shorter computation times [12]. However, despite these advantages, the averaging of turbulent fluctuations introduces an additional unknown quantity – the Reynolds stress tensor, which requires a turbulence model to close the resulting system of equations.

According to the classical Reynolds decomposition, the instantaneous value of any flow variable is represented as the sum of a mean component and a fluctuating component. By applying this decomposition to an arbitrary variable and using the properties of averaging and commutativity, one obtains the Reynolds-averaged Navier-Stokes (RANS) equations as

$$\rho\overline{u}_j\frac{\partial\overline{u}_i}{\partial x_j}=-\frac{\partial\overline{p}}{\partial x_i}+\mu\frac{\partial^2\overline{u}_i}{\partial^2 x_j}-\rho\frac{\partial\overline{u_i'u_j'}}{\partial x_j}. \quad (3)$$

In equation (3) the last term contains the Reynolds stress tensor, which describes the transport of momentum by velocity fluctuations and necessitates closure of the RANS system. Taking into account the Reynolds-averaged Navier-Stokes equations, one obtains the continuity equation, three equations for the components of the mean velocity, and the components of the Reynolds stress tensor. As a result, there are ten unknown functions: the components of the mean velocity, the mean pressure, and the diagonal and off-diagonal components of the Reynolds stress tensor. This yields four equations and ten unknowns, so a closed system of equations cannot be obtained by simple averaging of the Navier-Stokes equations.

To overcome this difficulty, the Boussinesq hypothesis is employed, which is analogous to the Newtonian constitutive relation for a linearly viscous fluid. In this approach, the turbulent stresses are related to the mean strain-rate tensor through a scalar quantity, the turbulent (eddy) viscosity, which in turn depends on the local state of turbulence. In other words, the turbulent stresses are assumed to be proportional to the gradients of the mean velocities.

For numerical simulation of aerodynamic parameters in dedicated CFD software such as Ansys Fluent, it is convenient to use a generic transport equation, in which the transport of momentum and energy is represented by diffusion-like terms:

$$\frac{\partial(\rho\varphi)}{\partial t}+\frac{\partial(\rho\varphi u)}{\partial x}+\frac{\partial(\rho\varphi v)}{\partial y}+\frac{\partial(\rho\varphi w)}{\partial z}=\frac{\partial}{\partial x}\left(\Gamma\frac{\partial\varphi}{\partial x}\right)+\frac{\partial}{\partial y}\left(\Gamma\frac{\partial\varphi}{\partial y}\right)+\frac{\partial}{\partial z}\left(\Gamma\frac{\partial\varphi}{\partial z}\right)+S_\varphi, \quad (4)$$

where $\varphi$ – common variable; $u$ – velocity component on the $x$-axis, $\mathrm{ms}^{-1}$; $v$ – velocity component on the $y$-axis, $\mathrm{ms}^{-1}$; $w$ – velocity component on the $z$-axis, $\mathrm{ms}^{-1}$; $k$ – turbulent kinetic energy, J; $\varepsilon$ – turbulent dissipation; $\Gamma$ – generalized diffusion coefficient; $S_\varphi$ – generalized source term.

In differential form, such a universal transport equation can be written as a balance of transient, convective, diffusive, and source terms for an arbitrary transported quantity.

Accurate numerical simulation of the aerodynamic behaviour of a high-speed elevator car requires the selection of a turbulence modelling approach that can provide high prediction accuracy within feasible computational resources. In this context, we focus on two-equation turbulence models, which introduce two additional transport equations. The Standard $k$-$\varepsilon$ turbulence model is widely used for fully developed turbulent flows and free shear jets due to its relatively low parameterization complexity and robust convergence behavior [13]. However, it exhibits large errors and poor physical fidelity in near-wall regions and flow separation zones around streamlined bodies, particularly in the presence of strong adverse pressure gradients.

Well-known modifications of this model, such as the RNG and Realizable $k$-$\varepsilon$ models, offer improved performance for swirling and curved turbulent flows by altering the form of the dissipation-rate equation and the formulation of the turbulent viscosity [14]. Despite these advantages, their near-wall treatment, like that of the baseline model, relies on wall function approaches and does not provide sufficiently accurate resolution of the boundary layer in complex flow configurations.

The interaction of a high-speed elevator car with the airflow inside the confined hoistway is governed by several factors, including flow constriction in the narrow clearances between the shaft and the car walls, separation and subsequent reattachment of turbulent flows, and the presence of a long, highly non-uniform wake. Solving this type of problem requires a detailed representation of both the external flow and the behaviour of the flow in near-wall regions, which can be achieved using the SST $k$-$\omega$ turbulence model. This approach employs blending functions to combine the advantages of the $k$-$\omega$ model in the near-wall region, where it can accurately resolve the boundary-

layer structure, with those of the *k*-ε model in the outer flow, where it is less sensitive to free-stream conditions and provides stable solutions [15].

Existing studies on the aerodynamic characteristics of streamlined bodies interacting with airflow in confined domains (such as high-speed trains and high-speed elevators) consistently indicate that the SST *k*-ω model provides the most accurate reproduction of pressure distributions and other aerodynamic parameters in problems involving multiple flow separations under crossflow conditions. In contrast, turbulence models of the *k*-ε family generally show a lower level of agreement between numerical predictions and experimental data for such flow configurations.

Thus, for the aerodynamic problem under consideration, involving high-speed elevators, the flow in the lateral and frontal clearances between the car surface and the shaft walls is characterized by strong flow constriction and the formation of a complex vortex structure with multiple separation and reattachment events. The most critical task is to obtain an accurate and detailed description of the flow behaviour in near-wall regions and in separation zones. To this end, we adopt the SST *k*-ω turbulence model, which offers an optimal compromise between the required computational resources and the accuracy of the predicted aerodynamic processes associated with elevator motion.

*2.2. Simulation modelling*

For the numerical simulations in the Ansys Fluent environment, which is based on the finite volume method, a typical model of a commercially produced high-speed elevator of Russian manufacture is employed. The overall dimensions of the elevator shaft, the clearances between the car walls and the shaft walls, as well as the height-related parameters, are adopted in accordance with the building specifications provided by the manufacturer. Figure 1 shows the computational model of the high-speed passenger elevator car with installed fairings, which represents a simplified version of the geometry of a standard elevator car. In the configuration without fairings, the car is formed by four straight side walls and two straight end walls.

The roof fairing of the elevator car is a structure consisting of longitudinal and transverse stiffening ribs covered with a continuous metal sheet with specified bend radii. In the present study, a series of simulation investigations is carried out to determine the optimal shape of the car fairing that combines maximum reduction of aerodynamic loads with feasibility for industrial manufacturing. The structural layout of the three-sided car fairing is shown in Figure 2. The combinations of fairing edge radii used in this study are given in Table 1.

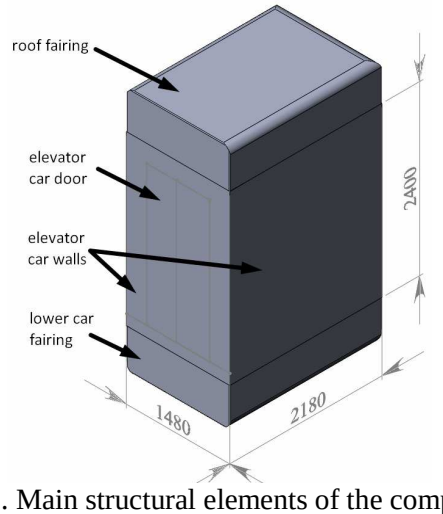



Fig. 1. Main structural elements of the computed elevator car model

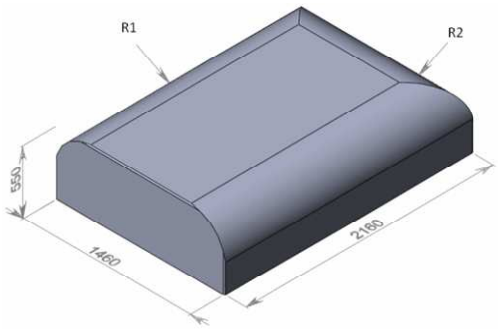



Fig. 2. Main structural elements of the computed elevator car model

Tab. 1. Geometric parameters of the elevator car fairings

| Computational scheme | Without the car fairing | Scheme A | Scheme B | Scheme C | Scheme D | Scheme E |
|---|---|---|---|---|---|---|
| Fillet radius R1, mm | 0 | 50 | 100 | 200 | 300 | 400 |
| Fillet radius R2, mm | 0 | 100 | 150 | 250 | 350 | 450 |

It is reasonable to perform the simulations on a scaled digital model of a real elevator at a 1:10 scale, which makes it possible to significantly reduce the required computational resources while preserving the physical similarity of the obtained results. The technical parameters of the elevator shaft and car under study are given in Table 2.

Tab. 2. Characteristics of the elevator computational model

| Parameter | Initial value | Value for the digital twin model |
|---|---|---|
| Cabin width W, mm | 1480 | 148 |
| Cabin depth D, mm | 2180 | 218 |
| Cabin height without fairing H, mm | 2400 | 240 |
| Shaft width Ws, mm | 2200 | 220 |
| Shaft depth Ds, mm | 2700 | 270 |
| Height of the investigated shaft section Hs, mm | 15000 | 1500 |

The car motion is analysed at a nominal speed of 4 m/s, with the airflow being modeled as an incompressible Newtonian fluid. As mentioned above, the SST *k*-ω turbulence model is employed. The physical properties of the fluid are specified to correspond to the operating conditions of passenger elevators in accordance with the relevant standards.

The computational setup represents the space confined by the shaft walls, inside which the elevator car moves. The shaft is divided into three characteristic zones: two zones located above and below the car, and a separate working zone containing the car. The zone above the car is associated with the development of the inlet flow and velocity profile, as well as with the growth of the boundary layer along the shaft walls. For this zone, a structured hexahedral mesh with uniform cell size is adopted, ensuring a homogeneous particle distribution at the inlet cross-section and preventing the generation of artificial disturbances. The working zone contains the critical region with the most complex airflow behaviour. The main difficulty here is the accurate resolution of boundary layers, where flow separation occurs and secondary flows develop. To capture this complex flow, a hybrid mesh is used: an unstructured tetrahedral mesh in the core flow region, which offers high flexibility and adaptability to the complex geometry of the car with fairings, combined with structured prismatic layers in the near-wall regions, enabling accurate prediction of boundary-layer parameters. In the zone below the car, by analogy with the upper zone, it is appropriate to employ a structured hexahedral mesh capable of accurately resolving the wake and the decay of the airflow. The resulting computational mesh is shown in Figure 3.

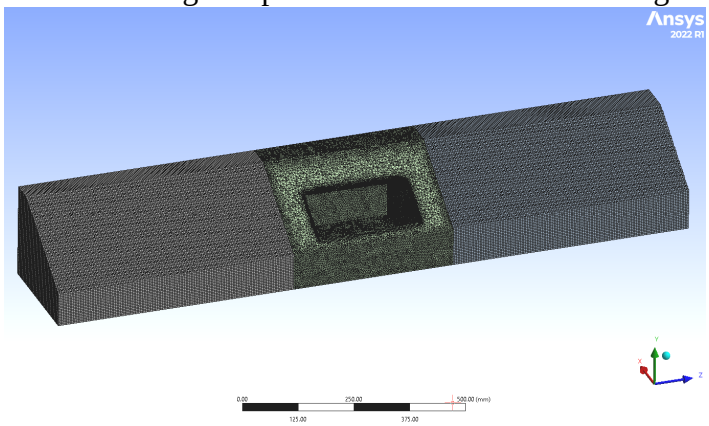



Fig. 3. Computational mesh describing the three zones of the model

The convergence of the simulation results is assessed using the following convergence criteria: 10-4 for the energy equation and 10-6 for the remaining variables (velocity, pressure, and turbulence). The spatial discretization schemes are selected according to the requirements of the problem: the PRESTO (pressure staggering option) scheme is used for pressure, due to the strongly convective nature of the flow; for momentum, turbulent kinetic energy, and specific dissipation rate, the high-resolution scheme is applied, which enables accurate resolution of turbulence and provides

an effective accuracy close to third order. In addition, under-relaxation factors are introduced, namely 0.7 for velocity, 0.3 for pressure, and 0.8 for the turbulent kinetic energy and specific dissipation rate.

*2.3. Numerical simulation results*

As a result of the simulation of six computational configurations of a high-speed passenger elevator car, including one baseline configuration without a fairing and five configurations with fairings of different geometric shapes (Table 1), a clear dependence of the car roof shape on the aerodynamic processes in the elevator shaft was identified. With increasing rounding radii of the fairings, a reduction in drag force and drag coefficient is observed, along with a decrease in pressure differences and velocity gradients, a modification of the turbulent flow structure, a shortening of the wake length, and changes in several other key aerodynamic parameters. At the same time, a diminishing-returns effect arises, whereby further increases in the fairing edge radii lead to a reduction in the incremental improvement of aerodynamic performance.

The baseline configuration without fairings is characterized by critical aerodynamic loads corresponding to an almost non-streamlined bluff rectangular body, which generates intense pairs of vortices with high turbulence levels, leading to the formation of a Karman vortex street with strong pressure and velocity fluctuations. This, in turn, results in vibration, noise, and reduced ride comfort for passengers. Configurations with rounded edges to varying degrees provide a noticeable beneficial effect, demonstrating the effectiveness of the proposed solution. The numerical simulation results are summarized in Table 3.

The most effective solution is scheme C, which has geometric characteristics intermediate between those of the other models. This configuration yields a 41% reduction in drag coefficient, a 77% reduction in the maximum turbulent kinetic energy $TKE_{\max}$, and a 54% reduction in the wake length. In addition, a fundamental change in the structure of the intense airflow is observed, namely the disappearance of the Karman vortex street, which is accompanied by a corresponding reduction in the adverse effects of noise and vibration on elevator passengers. Thus, the fairing with edge rounding $R_1$ = 200 mm and $R_2$ = 250 mm can be regarded as the optimal solution, both in terms of aerodynamic performance and feasibility of manufacturing under industrial conditions.

Tab. 3. Summary table of numerical simulation results

| Computational scheme | Without the car fairing | Scheme A | Scheme B | Scheme C | Scheme D | Scheme E |
|---|---|---|---|---|---|---|
| $C_D$ | 1.03 | 0.77 | 0.68 | 0.61 | 0.58 | 0.57 |
| $\Delta C_D$, % | - | -25.24 | -33.98 | -40.78 | -43.69 | -44.66 |
| $\Delta C_{p.base}$, % | ±0.051 | ±0.024 | ±0.017 | ±0.005 | ±0.003 | ±0.002 |
| $l_{rec}$, m | 2.0 | 1.35 | 1.05 | 0.92 | 0.71 | 0.63 |
| $\Delta l_{rec}$, % | - | -32.5 | -47.5 | -54 | -64.5 | -68.5 |
| $v_{\max1}$, m/s | 11.65 | 10.18 | 10.15 | 10.10 | 10.06 | 9.55 |
| $v_{\max2}$, m/s | 11.85 | 10.48 | 10.22 | 9.93 | 9.76 | 9.53 |
| $v_{\max3}$, m/s | 11.83 | 10.34 | 10.17 | 9.81 | 9.63 | 9.51 |
| $p_{\max3}$, m/s | 58.51 | 41.38 | 37.72 | 33.49 | 30.18 | 29.11 |
| $p_{\min3}$, m/s | -77.27 | -68.23 | -66.85 | -64.16 | -60.91 | -57.29 |
| $\Delta p$, Pa | 136.08 | 109.61 | 104.57 | 97.65 | 91.09 | 86.4 |
| $TKE_{\max}$, $m^2/s^2$ | 0.26 | 0.11 | 0.08 | 0.06 | 0.04 | 0.03 |
| $I_t$, % | 13.81 | 9.32 | 7.11 | 5.53 | 4.48 | 3.97 |

## 3. Experimental validation

For maximum accuracy of the obtained results, it was decided to carry out the experiment directly on a full-scale high-speed elevator operating under normal conditions in a test shaft, while maintaining geometric consistency between the parameters of the simulated model and the actual elevator installation. The aim of the experiment is to obtain reliable full‑scale data describing the

distribution of velocities and instantaneous pressure values of the turbulent airflow at various points, the aerodynamic characteristics, and associated ride-comfort indicators for passengers – namely, noise and vibration levels inside the car – for subsequent comparison and analysis. The following measured and investigated quantities are selected to enable a comprehensive comparison between the simulation and the experiment:

– Pressure difference. Differential pressure sensors are installed in the upper and lower parts of the car, corresponding to the stagnation zone of the incoming flow and the low-pressure region, respectively. These sensors record the static pressure difference between the lower and upper parts of the car with an accuracy better than ±1 Pa (Fig. 4, a).

– Vibration. Three-axis accelerometers are installed at the geometric centre of the car floor and at the approximate head level of elevator users to measure vibration accelerations over the frequency range 0.5-500 Hz (Fig. 4, b).

– Noise. The equivalent sound pressure level is measured using a precision sound level meter with a high-accuracy microphone. The microphone is positioned at a height of 20-50 cm above the car floor.

– For each configuration – with the optimally shaped fairing and without it – a series of at least five runs of the elevator at the nominal speed is performed in order to reduce the influence of random fluctuations. As a result of the experiments, averaged values of the target parameters are obtained; these are presented in Table 4.

Tab. 4. Comparison of numerical simulation and experimental results

| Parameter | Without the car fairing | Scheme C | Comparison of results | Maximum deviation from the numerical simulation |
|---|---|---|---|---|
| $\Delta p$, Pa | 126,55 | 91,3 | -27,85% | ~7% |
| $C_D$ | 1,1 | 0,66 | -40% | ~8% |
| $L_{A.eq}$, dBa | 57,9 | 51,8 | -10,54% | - |
| $a$, m/s$_2$ | 0,46 | 0,3 | -34,78% | ~8% |

The experimental results obtained for the car equipped with a fairing indicate that installing a fairing of special shape reduces the pressure difference on the car roof by approximately 28%, which corresponds to a decrease in the high-pressure region in the stagnation zone and a shortening of the recirculation zone. The vibration accelerations are reduced by about 35%, demonstrating a decrease in the fluctuating aerodynamic loads, which are one of the main sources of structural vibration of the elevator car. The noise level is reduced by 6.1 dB, down to 51.8 dB, which is consistent with the standard in-car noise limits for normal elevator operation.




a b

Fig. 4. Experimental study of the high-speed elevator: a – vibration measurement inside the elevator car; b – noise measurement inside the elevator car

## 4. Conclusion

Main objective of this study was to develop and validate an integrated approach to reducing the aerodynamic loads on a high-speed elevator car by combining mathematical modeling, numerical simulation, and experimental investigations. According to the comparison between the numerical simulation results and the experimental data for the specially optimized fairing shape, the discrepancies do not exceed 8% for the key aerodynamic and vibroacoustic parameters, which confirms the adequacy of the adopted mathematical model and the numerical simulation method.

The key scientific findings of this work can be summarized as follows:

– A mathematical model of the aerodynamic processes in a high-speed elevator shaft has been developed and substantiated. The classical Navier-Stokes equations for a viscous incompressible fluid were transformed into the Reynolds-averaged Navier-Stokes (RANS) equations using the Boussinesq hypothesis and a generic transport equation formulation as implemented in Ansys Fluent. It has been shown that, for characteristic car speeds on the order of 4 m/s and the relevant geometrical dimensions of the clearances, the airflow can be treated as incompressible, while the flow regime is governed by a high Reynolds number, which justifies the use of the SST $k$-$\omega$ turbulence model to accurately describe near-wall layers, multiple separations, and the vortex structure in the shaft clearances.

– A detailed numerical investigation of the influence of the elevator car fairing geometry has been carried out, and the optimal fairing shape has been identified. Based on the dimensions of a commercially produced high-speed elevator, a 1:10 scaled computational model of the shaft and car was constructed, and the configuration of the computational domain and hybrid mesh was defined, ensuring adequate resolution of the boundary layer and wake. For the baseline car without a fairing and five fairing variants of different shapes, pressure and velocity fields were obtained, aerodynamic coefficients and unsteadiness characteristics of the flow were determined, and it was established that the three-sided fairing of Scheme C provides up to a 41% reduction in drag coefficient, a reduction in turbulent kinetic energy in the wake of up to 77%, and a substantial shortening of the recirculation region, while maintaining manufacturability and feasibility under industrial production conditions.

– The effectiveness of the developed fairing has been experimentally confirmed, and the numerical simulation results have been validated. Full-scale tests of the high-speed elevator were carried out in a test shaft whose geometry matched that of the computational model, and measurements of pressure difference, vibration accelerations, and noise level inside the car were performed for configurations with and without the fairing. It was shown that installing the Scheme C fairing leads to a 28-37% reduction in the pressure difference on the car roof, a reduction of approximately 30-36% in vertical vibration accelerations, and a 6-7 dBA decrease in noise level down to standard-compliant values, while the discrepancies between the numerical and experimental data for the monitored parameters do not exceed 8%. This allows the proposed fairing geometry to be regarded as an engineeringly mature solution that is ready for practical implementation in the design and modernization of high-speed elevators.

**Список литературы**


1. Парусов А.А., Шарапов Р.Р. Анализ шумовых характеристик при движении скоростного лифта // Известия Тульского государственного университета. Технические науки. – 2024. – №12. – С. 398-401. – doi.org/10.24412/2071-6168-2024-12-398-399.
2. Парусов А.А., Шарапов Р.Р. Разработка конструкции обтекателя кабины скоростного лифта на основании результатов CFD-моделирования // Известия Тульского государственного университета. Технические науки. – 2025. – №12. – С. 402-408. – doi.org/10.24412/2071-6168-2025-12-402-403.

3-15. См. *References.*


**References**


1. Parusov A.A., Sharapov R.R. Analysis of noise characteristics during high-speed lift movement // News of the Tula state university. Technical sciences. 2024, vol. 12, pp. 398-401. doi.org/10.24412/2071-6168-2024-12-398-399.
2. Parusov A.A., Sharapov R.R. Development of a high-speed elevator cabin fairing design based on CFD modeling result // News of the Tula state university. Technical sciences. 2025, vol. 12, pp. 402-408. doi.org/10.24412/2071-6168-2025-12-402-403.

3. Lee S., Cheong C., Kim J., Kim B.-h. Numerical Analysis and Characterization of Surface Pressure Fluctuations of High-Speed Trains Using Wavenumber–Frequency Analysis // Applied Sciences. 2019, vol. 9, no. 22, p. 4924. doi.org/10.3390/app9224924.
4. Cross D., Hughes B., Ingham D., Ma L. Enhancing the piston effect in underground railway tunnels // Tunnelling and Underground Space Technology. 2017, vol. 61, pp. 71-81. doi.org/10.1016/j.tust.2016.10.001.
5. Ricco P., Baron A., Molteni P. Nature of pressure waves induced by a high-speed train travelling through a tunnel // Journal of Wind Engineering and Industrial Aerodynamics. 2007, vol. 95, no. 8, pp. 781-808. doi.org/10.1016/j.jweia.2007.01.008.
6. Bai H., Shen G., So A. Experimental-based study of the aerodynamics of super-high-speed elevators // Experimental-based study of the aerodynamics of super-high-speed elevators. Building Services Engineering Research & Technology. 2005, vol. 26, no. 2, pp. 129-143. doi.org/10.1191/0143624405bt121oa.
7. Jun Z., Manman L., Minzong L., Bei L., Shenxin J., Lei Q., Jiancheng M., Hong Z., Lei X. Simulation and experimental study on the aerodynamic characteristics of a high-speed elevator with three-sided arc fairings // Journal of Building Engineering. 2024, vol. 81. doi.org/10.1016/j.jobe.2023.108172.
8. Jun Z., Manman L., Minzong L., Bei L., Shenxin J., Lei Q., Jiancheng M., Hong Z., Lei X. Research on the Aerodynamic Characteristics of an Ultrahigh-speed Elevator During the Staggering Process Between the Car and Counterweight // Journal of Applied Fluid Mechanics. 2025, vol. 18, pp. 1158-1173. doi.org/10.47176/jafm.18.5.3140.
9. Jun Z., Manman L., Minzong L., Bei L., Shenxin J., Lei Q., Jiancheng M., Hong Z., Lei X. Aerodynamic characteristics of a super high-speed elevator with different toe guards // Journal of Wind Engineering and Industrial Aerodynamics. 2023, vol. 223, p. 105292. doi.org/10.1016/j.jweia.2022.105292.
10. Shi L.Q., Liu Y.Z., Jin S.Y. Numerical simulation of unsteady turbulent flow induced by two-dimensional elevator car and counter weight system // Journal of Hydrodynamics. 2007, vol. 19, pp. 720-725. doi.org/10.1016/S1001-6058(08)60009-8.
11. Cui H., Zhang Q., Zhang R., Zhang L. Research on aerodynamic and flow field characteristics of high speed elevator with different shaft blockage ratio // Journal of Physics Conference Series. 2020, vol. 1653, p. 012024. doi.org/10.1088/1742-6596/1653/1/012024.
12. Qiao S., Zhang R.Z., He Q. Theoretical modeling and sensitivity analysis of the car-induced unsteady airflow in super high-speed elevator // Journal of Wind Engineering and Industrial Aerodynamics. 2019, vol. 188, pp. 280-293. doi.org/10.1016/j.jweia.2019.02.012.
13. Cheng Y., Lien F.S., Yee E., Sinclair R. A comparison of large Eddy simulations with a standard k–ε Reynolds-averaged Navier–Stokes model for the prediction of a fully developed turbulent flow over a matrix of cubes // Journal of Wind Engineering and Industrial Aerodynamics. 2003, vol. 91, no. 11, pp. 1301-1328. doi.org/10.1016/j.jweia.2003.08.001.
14. Mompean G. Numerical simulation of a turbulent flow near a right-angled corner using the Speziale non-linear model with RNG K–ε equations // Computers & Fluids. 1998, vol. 27, no. 7, pp. 847-859. doi.org/ 10.1016/S0045-7930(98)00004-8.
15. Mozaffari S., Cai S-G Jacob J., Sagaut P. Lattice Boltzmann k-ω SST based hybrid RANS/LES simulations of turbulent flows // Journal of Computational Physics. 2024, vol. 514. doi.org/10.1016/j.jcp.2024.113269.

*Сведения об авторах:* *Information about authors:*

| | |
|---|---|
| **Парусов Андрей Андреевич –** аспирант | **Parusov Andrei Andreevich –** postgraduate student |
| **Шарапов Рашид Ризаевич –** доктор технических наук, профессор кафедры Механизации, автоматизации и роботизации строительства | **Sharapov Rashid Rizaevich –** Doctor of Technical Sciences, Professor of the Department of Mechanization, Automation and Robotization of Construction |
| parus1@mail.ru | |

*Получена 09.09.2026*